J Eng Math (2007) 58:301–315
DOI 10.1007/s10665-006-9130-6

Optimal-control theory applied to ship maneuvering in restricted waters

Brian S. Thomas · Paul D. Sclavounos

Received: 6 February 2006 / Accepted: 21 December 2006 / Published online: 27 February 2007

Abstract Ship drivers have long understood that powerful interaction forces exist when ships operate in close proximity to rigid boundaries or other vessels. Controlling the effects of these forces has been traditionally handled by experienced helmsmen. The purpose of this study is to apply modern optimal-control theory to such maneuvering scenarios in order to show that helmsmen may some day be replaced by modern controllers. The maneuvering equations of motion are cast in a linear state-space framework, permitting the design of a linear quadratic (LQ) controller. The hydrodynamic effects are modeled using potential-flow theory in order to simulate the interaction forces and test the performance of the controller. This study demonstrates that the linear quadratic regulator effectively controls ship motions due to the presence of a boundary or other vessel over a broad range of speeds and separation distances. Viscous effects are modeled by equivalent linearization and, when compared to the effective damping introduced by the controller, are shown to be insignificant.

Keywords Linear-quadratic-Gaussian regulators · Ship maneuvering · Ship navigation in restricted waters

1 Introduction

The problem of controlling ships during their passages at sea has a history as old as human maritime endeavors. The past century saw great advances in control theory. The age-old marine problems were among the first applications to benefit from these innovations. Notably marine autopilots were a primary test bed as feedback control systems were beginning to be formalized in a mathematical setting during the early 1900s. In today's age of ever-faster paced, higher-efficiency operations, a strong focus on optimal routing and collision avoidance has emerged and the current control-theory literature has numerous examples of the sophisticated work going on in this area. Research, however, appears to be less extensive on the effect of inter-vessel interaction forces and their use in the design of robust controllers. This is the subject of the present study.

B. S. Thomas · P. D. Sclavounos (✉)
Department of Mechanical Engineering, Massachusetts Institute of Technology, Cambridge, MA 02139-4307, USA
e-mail: pauls@mit.edu

1.1 The hydrodynamic problem

The interaction forces that develop between ships and banks in restricted waters have been understood on a practical level by mariners for centuries. Masters of large vessels take pains to keep prudent distances between vessels in order to moderate these forces.

In contrast to the wealth of practical knowledge of these phenomena and how best to control them, quantitative approaches are still relatively scarce. Model tests and full-scale analyses have been conducted on a limited basis, and *Principles of Naval Architecture* [1], treats the subject in some detail. More recently model tests have been reported on by Vantorre et al. [2] for a variety of overtaking scenarios by ships of differing geometries. This work was primarily intended for improving the accuracy of training simulators; however, its application to the control problem could be significant. Analytically, the most general work on this subject was undertaken by Tuck and Newman in 1974 [3]. Using slender-body theory they propose a set of equations to evaluate the hydrodynamic forces and moments between two slender bodies on parallel courses but with arbitrary speed, separation, and stagger. This model, although only in moderate agreement with empirical results, can be useful in formulating and simulating control problems involving ship–ship interactions.

1.2 The control problem

The ship-maneuvering problem contains strongly coupled dynamics of the ship sway and yaw modes of motion. This coupling requires a multiple-input multiple-output (MIMO) approach to the control problem. Modern state-space methods provide such a method. These state-space methods minimize some cost, typically the deviation from a desired state and control usage, while subject to the constraints of the dynamics of the system. The popular linear quadratic (LQ) family of controllers take their name from the linearity of their state equation and the quadratic form of their cost function. One particular advantage of the LQ optimal-control framework used here is that the existence of a solution to the problem guarantees both optimality and stable control. The robustness properties of LQ controllers are favorable enough to make them popular in a variety of applications, notably aircraft control.

This paper will address the specific maneuvering problem of a ship traveling next to a bank or its image. It will be shown that this problem generates a sway force and yaw moment in general, which make the system unstable. Ships typically control their motions by altering speed and rudder angle. For the bank-suction problem it will be shown with an appropriate potential-flow model that the magnitudes of the interaction forces are dependent on forward speed. Completely eliminating the effect of the bank through speed change means stopping completely, which is clearly not reasonable. Alternatively, applying a rudder angle generates both a sway force and yaw moment. For a ship proceeding parallel to a wall, a heuristic argument can be made that steady motion with constant separation requires that the force and moment generated by a constant rudder must exactly balance the interaction force and moment. This is not possible in the general case and so an LQ controller design has been developed. The benefit of using optimal-control theory in this case is that the system's dynamical properties are central to the controller-design process. The controller's 'knowledge' of this dynamics allows it to find an equilibrium between control, hydrodynamic and interaction forces. This equilibrium is demonstrated with a numerical simulation. In addition, the relative importance of viscous forces has been addressed. Equivalent linearization for small sway and yaw motions allows viscous-damping terms to be applied to the controlled system. The simulation demonstrates that the viscous-damping terms are much smaller than the damping introduced by the controller and are thus negligible.

2 The hydrodynamic model

2.1 Overview

The goal of this hydrodynamic model is to determine the steady and unsteady hydrodynamic forces and moments exerted on a vessel due to the presence of another vessel or a vertical wall. The method of images is used to simulate the case where a ship is traveling parallel to a vertical boundary.

In the present study the 3D Rankine panel method SWAN (Ship Wave ANalysis) developed at MIT's Laboratory for Ship and Platform Flows was used to evaluate the appropriate hydrodynamic quantities. More details on SWAN are presented in [4].

2.2 The mathematical model

The 3D potential-flow problem is commonly expressed as a boundary-value problem for the velocity potential ϕ. In the present analysis the free surface is considered rigid. This approximation leads to the classic "double body" flow.

The steady pressure distribution and resulting suction sway force and yaw moment follow from Bernoulli's equation in terms of the steady double-flow potential ϕ_1 arising from the ship forward motion:

$$p = -\frac{1}{2}\rho\left(\nabla\phi_1 \cdot \nabla\phi_1\right) + \rho U \phi_{1x}, \tag{1}$$

$$\vec{F} = \iint_{S_B} p\,\vec{n}\,\mathrm{d}S, \tag{2}$$

$$\vec{M} = \iint_{S_B} p\left(\vec{x} \times \vec{n}\right)\mathrm{d}S. \tag{3}$$

The added-mass tensor follows from the classical expression

$$m_{ij} = \rho \iint_{S_B} \phi_i n_j \mathrm{d}S, \tag{4}$$

where ϕ_i is the unit double-body potential due to the ith mode of motion of the vessel next to a vertical wall and $n_j,\ j = 1,\ldots,6$ are the unit vectors on the ship boundary pointing out of the fluid domain.

2.3 Numerical results for a ship-like body

Figure 1 displays a fore–aft asymmetric hull geometry with semi-circular cross-sections. For this body a yawing moment will result due to the longitudinal asymmetry of the flow. In addition, the sway–yaw cross-coupling added-mass coefficient m_{26} will be non-zero.

Figure 2 displays the steady sway-suction force and yaw moment as a function of the ship distance from the wall computed by SWAN. As expected, both force and moment decrease rapidly with increasing distance from the wall. Figure 3 plots the sway–yaw added-mass coefficients computed by SWAN, illustrating their dependence on the ship distance from the wall.

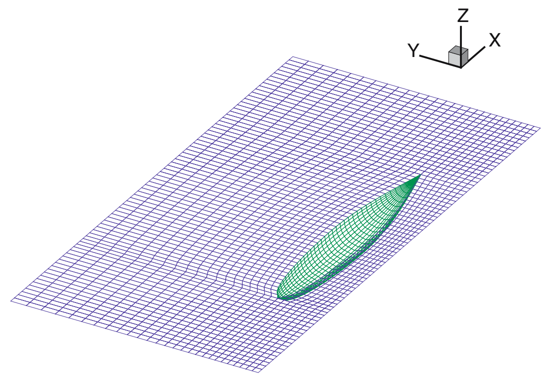

Fig. 1 SWAN domain mesh (asymmetric body)

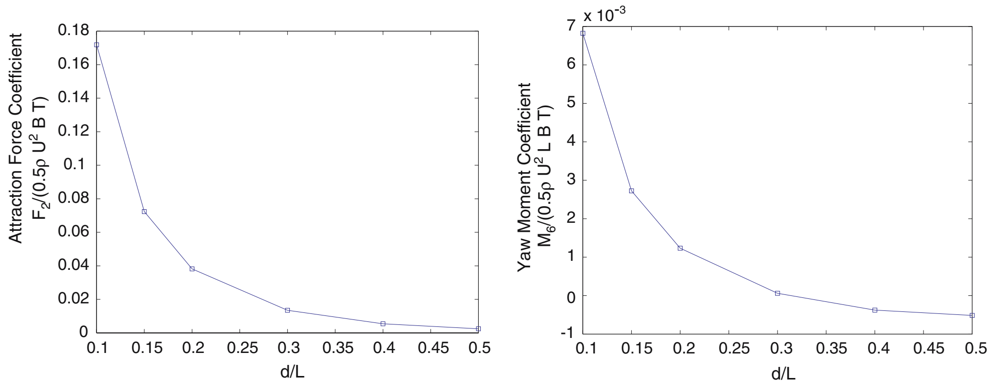

Fig. 2 SWAN results for the attraction force and bow-out moment for an asymmetric body

3 Maneuvering equations

3.1 Ship-maneuvering fundamentals

We begin with the purely inertial properties of the ship, with Δ being its displacement and I_z its yaw moment of inertia. The hydrodynamic sway force (F_2) and yaw moment (M_3) arising from the ship sway and yaw velocity and acceleration U_2,$\dot{U}_2$ and Ω_3, $\dot{\Omega}_3$ follow from Newton's law as follows:

$$F_2(U_2,\dot{U}_2,\Omega_3,\dot{\Omega}_3) = \Delta(\dot{U}_2 - U_1\dot{\psi}), \quad M_3(U_2,\dot{U}_2,\Omega_3,\dot{\Omega}_3) = I_z\ddot{\Omega}_3. \tag{5}$$

Assuming small sway–yaw perturbation velocities and accelerations around the mean ship trajectory, we may approximate the above equations by linear expressions using Taylor's theorem. Ignoring the coupling between the surge and sway–yaw modes, we obtain the following expression:

$$\begin{aligned} \Delta(\dot{U}_2 - U_1\Omega_3) &= U_2\frac{\partial F_2}{\partial U_2} + \dot{U}_2\frac{\partial F_2}{\partial \dot{U}_2} + \Omega_3\frac{\partial F_2}{\partial \Omega_3} + \dot{\Omega}_3\frac{\partial F_2}{\partial \dot{\Omega}_3}, \\ I_z\dot{\Omega}_3 &= U_2\frac{\partial M_3}{\partial U_2} + \dot{U}_2\frac{\partial M_3}{\partial \dot{U}_2} + \Omega_3\frac{\partial M_3}{\partial \Omega_3} + \dot{\Omega}_3\frac{\partial M_3}{\partial \dot{\Omega}_3}. \end{aligned} \tag{6}$$

Assuming that a small rudder angle δ_R is applied, we may include the linear sway and yaw force and moment generated. Now the equations for the sway and yaw perturbation displacements are governed by the matrix equation

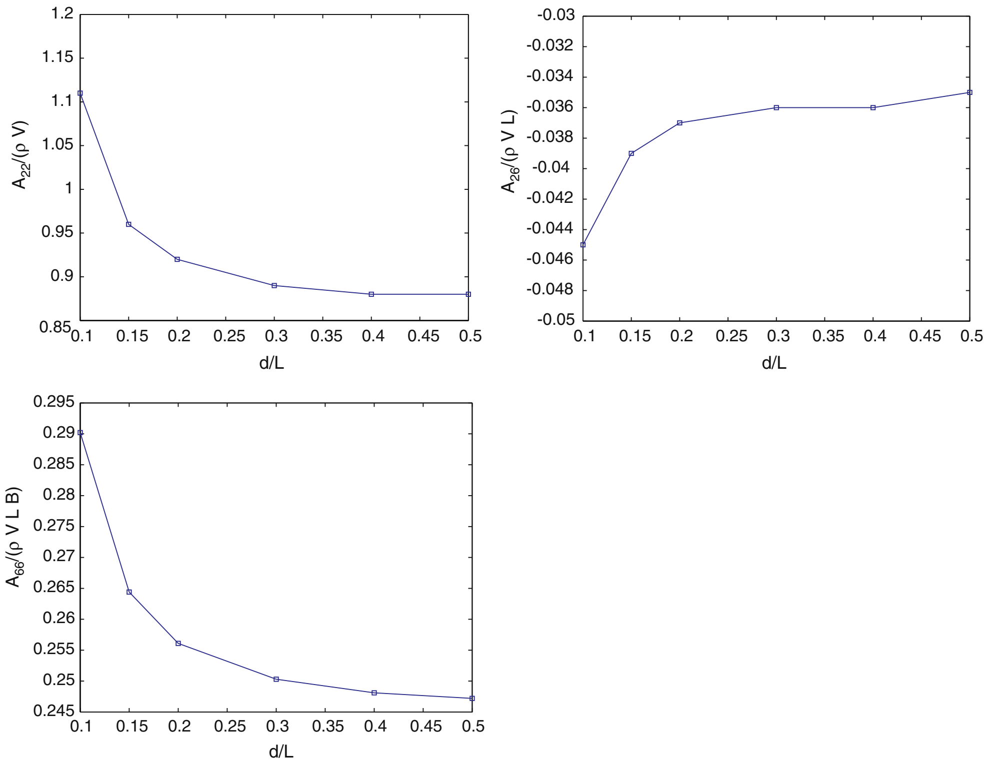

Fig. 3 SWAN results for the added mass and moments for an asymmetric body

$$\begin{bmatrix} -\dfrac{\partial F_2}{\partial \dot{U}_2}+\Delta & -\dfrac{\partial F_2}{\partial \dot{\Omega}_3} \\ -\dfrac{\partial M_3}{\partial \dot{U}_2} & -\dfrac{\partial M_3}{\partial \dot{\Omega}_3}+I_z \end{bmatrix} \begin{bmatrix} \dot{U}_2 \\ \dot{\Omega}_3 \end{bmatrix} = \begin{bmatrix} \dfrac{\partial F_2}{\partial U_2} & \left(\dfrac{\partial F_2}{\partial \Omega_3}-\Delta U_1\right) \\ \dfrac{\partial M_3}{\partial U_2} & \dfrac{\partial M_3}{\partial \Omega_3} \end{bmatrix} \begin{bmatrix} U_2 \\ \Omega_3 \end{bmatrix} + \begin{bmatrix} \dfrac{\partial F_3}{\partial \delta_R} \\ \dfrac{\partial M_3}{\partial \delta_R} \end{bmatrix} [\delta_R]. \tag{7}$$

In the present context, small deviations of the ship from its mean course are assumed. Therefore, the linear form of the Eq. 7 is acceptable for our purposes.

3.2 Hydrodynamic derivatives

In order to estimate the hydrodynamic derivatives present in Eq. 7, we turn to classic potential-flow theory. The equations for the force and moment on a moving body in an infinite and inviscid fluid and irrotational flow are presented by Newman [5]:

$$F_j = -\dot{U}_i m_{ji} - \varepsilon_{jkl} U_i \Omega_k m_{li}, \qquad M_j = -\dot{U}_i m_{j+3,i} - \varepsilon_{jkl} U_i \Omega_k m_{l+3,i} - \varepsilon_{jkl} U_i U_k m_{li}. \tag{8}$$

In these equations the index i goes from 1,. . .,6, while j, k, l can only take values 1,2,3. U_i is the velocity in the three rectilinear modes of motion, Ω_k are the three angular velocities, and ε_{jkl} is the alternating tensor. In our case, only the sway (U_2), yaw (U_6, Ω_3) and surge (U_1) modes are of interest, as all other velocities are assumed to be zero. In addition, the perturbation surge force (F_1) is assumed negligible compared to the propeller thrust required to maintain the steady forward velocity of the ship. Based on these assumptions

Fig. 4 Coordinate system

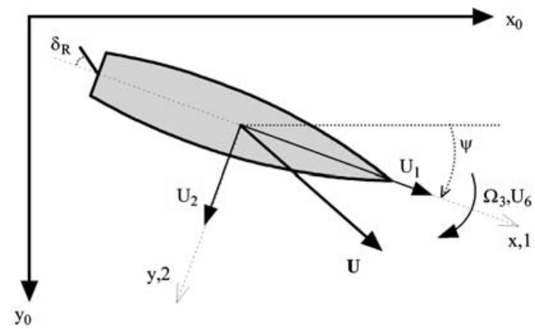

we may now determine the sway and yaw perturbation hydrodynamic force and moment F_2 and M_3:

$$F_2 = -\dot{U}_2 m_{22} - \dot{\Omega}_3 m_{26} - U_1 \Omega_3 m_{11}, \qquad M_3 = -\dot{U}_2 m_{62} - \dot{\Omega}_3 m_{66} + U_1 U_2 (m_{11} - m_{22}) - \Omega_3 U_1 m_{26}. \tag{9}$$

If the ship forward velocity U_1 in the x-direction is assumed constant, these two equations provide desired expressions for the hydrodynamic derivatives required in the maneuvering equations (Fig. 4). It follows that

$$\begin{aligned}
&\frac{\partial F_2}{\partial U_2} = 0, \quad \frac{\partial M_3}{\partial U_2} = U_1(m_{11} - m_{22}),\\
&\frac{\partial F_2}{\partial \Omega_3} = -U_1 m_{11}, \quad \frac{\partial M_3}{\partial \Omega_3} = -U_1 m_{26},\\
&\frac{\partial F_2}{\partial \dot{U}_2} = -m_{22}, \quad \frac{\partial M_3}{\partial \dot{U}_2} = -m_{62},\\
&\frac{\partial F_2}{\partial \dot{\Omega}_3} = -m_{26}, \quad \frac{\partial M_3}{\partial \dot{\Omega}_3} = -m_{66}.
\end{aligned} \tag{10}$$

With the derivatives so defined, Eq. 7 may be rewritten in terms of the known added-mass coefficients:

$$\begin{bmatrix} m_{22} + \Delta & m_{26} \\ m_{62} & m_{66} + I_z \end{bmatrix} \begin{bmatrix} \dot{U}_2 \\ \dot{\Omega}_3 \end{bmatrix} = \begin{bmatrix} 0 & -U_1(m_{11} + \Delta) \\ -U_1(m_{22} - m_{11}) & -U_1 m_{26} \end{bmatrix} \begin{bmatrix} U_2 \\ \Omega_3 \end{bmatrix} + \begin{bmatrix} F_R \\ M_R \end{bmatrix} [\delta_R]. \tag{11}$$

4 Control

4.1 Optimal-control problem

Stengel [6] covers the derivation of the Linear Quadratic Regulator (LQR) and that derivation will not be repeated here. However, the basic problem is to minimize some quadratic cost function J constrained by the dynamics of the system. The system dynamics are contained in the state equation:

$$\dot{\mathbf{x}} = \mathbf{A}\mathbf{x} + \mathbf{B}\mathbf{u} + \mathbf{D}. \tag{12}$$

In this equation $\mathbf{x}$ is the state vector, $\mathbf{u}$ is the control vector, and $\mathbf{D}$ is a matrix containing disturbances to the system. $\mathbf{A}$ is the plant matrix obtained from the derivation of the equations of motion. $\mathbf{B}$ is an input matrix, stating the linear law that states the effect of the control parameters $\mathbf{u}$ upon the state vector $\mathbf{x}$.

The quadratic cost function takes the form:

$$J = \frac{1}{2}\int_0^T \left(\mathbf{x}^T\mathbf{Q}\mathbf{x} + \mathbf{u}^T\mathbf{R}\mathbf{u}\right)\mathrm{d}t. \tag{13}$$

Here $\mathbf{Q}$ is a positive semi-definite matrix containing the costs associated with deviations from the desired mean value of the state. $\mathbf{R}$ is a positive-definite matrix containing the costs associated with the control usage.

With the problem defined as above, the linear quadratic regulator now states that $\mathbf{u}(t)$ is the optimal-control trajectory provided that:

$$\mathbf{u}(t) = -\mathbf{R}^{-1}\mathbf{B}\mathbf{P}\mathbf{x}(t), \tag{14}$$

where $\mathbf{P}$ is the solution to the algebraic matrix Riccati equation,

$$0 = \mathbf{P}\mathbf{A} + \mathbf{A}^T\mathbf{P} - \mathbf{P}\mathbf{B}\mathbf{R}^{-1}\mathbf{B}^T\mathbf{P} + \mathbf{Q}. \tag{15}$$

Conventionally, the control law is stated in a compact matrix form as follows:

$$\mathbf{u}(t) = -\mathbf{K}\mathbf{x}(t), \tag{16}$$

where

$$\mathbf{R}^{-1}\mathbf{B}\mathbf{P} = \mathbf{K}. \tag{17}$$

Here $\mathbf{K}$ is known as the gain matrix, and is constant for constant time-invariant $\mathbf{A}$ and $\mathbf{B}$ matrices. Therefore, $\mathbf{K}$ may be calculated a priori and used throughout the system's operation.

4.2 The state equation for the steady case

Now the equations of motion from the previous section may be rewritten for the steady case where U_1 is considered to be a constant. The unsteady case where the forward speed is allowed to vary slowly in time and used as a control will be treated later. For compactness we introduce the following definitions:

$$\mathbf{m}_{ij} = \begin{bmatrix} \Delta + m_{22} & M_{26} + m_{26} \\ M_{26} + m_{26} & I_z + m_{66} \end{bmatrix}, \tag{18}$$

$$\mathbf{b}_{ij} = \begin{bmatrix} -U_1 m_{22}(x_T) & U_1(x_T m_{22}(x_T) - \Delta) \\ -U_1(m_{22} + x_T m_{22}(x_T)) & U_1(M_{26} + m_{26} - x_T^2 m_{22}(x_T)) \end{bmatrix}, \tag{19}$$

$$\mathbf{F}_R = \begin{bmatrix} \frac{1}{2}\rho U_1^2 S \frac{\partial C_L}{\partial \delta_R} \\ \frac{1}{2}\rho U_1^2 S \frac{\partial C_L}{\partial \delta_R} x_T \end{bmatrix}. \tag{20}$$

The state equation follows in the form:

$$\begin{bmatrix} \dot{U}_2 \\ \dot{\Omega}_3 \\ \dot{\psi} \\ \dot{y} \end{bmatrix} = \begin{bmatrix} \mathbf{m}_{ij}^{-1} & \cdot\mathbf{b}_{ij} & \begin{matrix} 0 \\ 0 \end{matrix} & \begin{matrix} 0 \\ 0 \end{matrix} \\ 0 & 1 & 0 & 0 \\ 1 & 0 & U_1 & 0 \end{bmatrix} \begin{bmatrix} U_2 \\ \Omega_3 \\ \psi \\ y \end{bmatrix} + \begin{bmatrix} \mathbf{m}_{ij}^{-1} & \cdot\mathbf{F}_R \end{bmatrix} [\delta_R], \tag{21}$$

where ψ is the ship yaw angular displacement and y its sway displacement from their zero mean values.

4.3 Forward speed as a control

The control problem is now extended to the more realistic scenario where speed is also allowed to vary. For large vessels, speed changes occur very slowly due to their large inertia. However, small changes in speed may have significant effects on the forces and moments and should not be neglected. The attraction force and moment generated by the presence of another vessel or boundary are dependent on both separation distance and forward speed. These forces and moments are expressed in the following form:

$$F_2 = \frac{1}{2} C_s(d) \rho BTU^2, \quad M_3 = \frac{1}{2} C_m(d) \rho BTLU^2. \tag{22}$$

Here L, B, and T are the length, beam and draft of the vessel, respectively. Now, if U is considered to be the sum of the initial forward velocity and a small perturbation $(U_1 + \delta_u)$, the equations become:

$$F_2 = \frac{1}{2} C_s(d) \rho BT(U_1^2 + 2U_1\delta_u + \delta_u^2), \quad M_3 = \frac{1}{2} C_m(d) \rho BTL(U_1^2 + 2U_1\delta_u + \delta_u^2). \tag{23}$$

The final term in this expression is of second order and can be neglected; however, the second term directly shows the effect of the perturbation velocity (δ_u) on the suction force and moment. Keeping only leading-order terms in the perturbation, we have

$$F_2 = C_s(d) \rho BTU_1\delta_u, \quad M_3 = C_m(d) \rho BTLU_1\delta_u. \tag{24}$$

These equations contain the effect of the forward speed variation on the side force and moment of interest.

Looking now at the effect of the perturbation velocity on the rudder forces and moments, we see that the same analysis may be applied:

$$F_R = \frac{1}{2} \rho S \frac{\partial C_L}{\partial \delta_R} \delta_R (U_1^2 + 2U_1\delta_u + \delta_u^2), \quad M_R = \frac{1}{2} \rho S x_T \frac{\partial C_L}{\partial \delta_R} \delta_R (U_1^2 + 2U_1\delta_u + \delta_u^2). \tag{25}$$

Since both δ_R and δ_u are small, there exist no first-order terms containing δ_u and so, to leading order, small speed changes will not affect the performance of the rudder.

With all of the above taken into account, the state equation may be stated in its complete form:

$$\dot{\mathbf{x}} = \mathbf{A}\mathbf{x} + \mathbf{B}\mathbf{u} + \mathbf{D}, \tag{26}$$

where,

$$\mathbf{A} = \begin{bmatrix} \mathbf{m}_{ij}^{-1} & \cdot\mathbf{b}_{ij} & \begin{matrix} 0 \\ 0 \end{matrix} & \begin{matrix} 0 \\ 0 \end{matrix} \\ 0 & 1 & 0 & 0 \\ 1 & 0 & U_1 & 0 \end{bmatrix}, \quad \mathbf{B} = \mathbf{m}_{ij}^{-1} \begin{bmatrix} \frac{1}{2}\rho U_1^2 S \frac{\partial C_L}{\partial \delta_R} & C_s(d)\rho BTU_1 \\ \frac{1}{2}\rho U_1^2 S \frac{\partial C_L}{\partial \delta_R} x_T & C_m(d)\rho BTLU_1 \end{bmatrix} \tag{27}$$

with $\mathbf{m}_{ij}$ and $\mathbf{b}_{ij}$ as defined in Eqs. 18 and 19. The state and control vectors are

$$\mathbf{x} = \begin{bmatrix} U_2 \\ \Omega_3 \\ \psi \\ y \end{bmatrix}, \quad \mathbf{u} = \begin{bmatrix} \delta_R \\ \delta_u \end{bmatrix}, \tag{28}$$

respectively. This set of state equations does not contain the body's forward speed, U_1, as a state variable. In order to remove this state variable, we have made certain assumptions. First, it is assumed that surge is not coupled to sway and yaw. Second, it is also assumed that, because the body is slender ($B/L \approx 0.15$), the surge added mass m_{11} is small compared to the ship mass. Finally, the main propulsive force is significantly greater than external hydrodynamic effects in surge.

4.4 Equivalent linear damping

Frequently viscous drag is approximated by a quadratic expression that is modeled by Morison's equation. In order to incorporate the quadratic force expressions into the linear model, drag must be linearized. It is here assumed that the ship sway and yaw motions may be expressed as oscillations about the ship mean path,

$$\xi_2 = |\Xi_2| \cos(\omega t + \varphi), \quad \xi_6 = |\Xi_6| \cos(\omega t + \varphi). \tag{29}$$

The goal is to develop an equivalent linear damping mechanism $B_{22_{\text{Visc}}}\dot{\xi}_2$ which dissipates the same amount of energy per cycle as the quadratic damping obtained from the application of Morison's equation. The resulting expressions for the linear sway and yaw damping coefficients are:

$$B_{22_{\text{Visc}}} = \frac{4\rho C_D A_P}{3\pi} \omega |\Xi_2| \tag{30}$$

and similarly for yaw:

$$B_{66_{\text{Visc}}} = \frac{4\rho C_D M_P}{3\pi} \omega |\Xi_6|. \tag{31}$$

The definition of the frequency ω, drag coefficient C_D, sway projected area A_P and yaw projected area second moment M_P are discussed below.

Table 1 Symmetric body characteristics

Length (L)	100 m
Beam (B)	15 m
Draft (T)	7.5 m
C_b	0.52
Rudder area (S)	18.75 m^2
$\frac{\partial C_L}{\partial \delta_R}$	4.71

5 Control-system simulation

5.1 Overview

In order to test the viability of the control system under consideration, a numerical simulation of the maneuvering problem was carried out. Namely, a vessel was modeled traveling next to a solid boundary in infinite depth. Utilizing the linear equations of motion derived previously and the hydrodynamic properties calculated by SWAN, the motion of the body was calculated for a variety of scenarios.

The simulation program, written with MATLAB, uses the state equation and the hydrodynamic properties generated by the hydrodynamic model to calculate the gain matrix **K**. Through the control law the controller specifies the control vector **u** in terms of the contemporaneous value of the state vector **x**. The force model sums the control, attraction and disturbance forces and applies them to the right-hand side of the maneuvering equations of motion.

5.2 Rudder modeling

While rudder sizes and shapes vary greatly with the purpose of the vessel, a rudder planform area (S) equal to 2.5% of the area of a rectangle formed by the vessel's length and draft is a good baseline estimate. If the rudder is modeled as a flat plate with a maximum span equal to the draft, in three dimensions the lift coefficient as a function of rudder angle (δ_R) may be approximated by the classical expression

$$C_L = \frac{2\pi \mathit{AR}}{\mathit{AR} + 2}\delta_R \tag{32}$$

Here AR is the effective aspect ratio. Because the free surface has been modeled as a rigid plane, it acts as a plane of symmetry. Thus, the aspect ratio of the rudder is effectively doubled to twice its conventional definition. The fundamental dimensions and rudder properties for the symmetric body are listed in Table 1.

5.3 Inherent system instability

Prior to applying the control, it is important to understand the system behavior in the absence of controls. Without the application of any controls the state equation simply becomes

$$\dot{\mathbf{x}} = \mathbf{A}\mathbf{x}. \tag{33}$$

If the solution to this equation may be cast in the form:

$$x(t) = c_1 \mathrm{e}^{\lambda t}, \tag{34}$$

Table 2 Maximum state and control values

$x_i$max	U_2	=	0.1 m/s
	Ω_3	=	0.57°/s
	ψ	=	5.7°
	y	=	0.1 m
	y_i	=	0.5 m·s
$u_i$max	δ_R	=	2.5°
	δ_u	=	0.25 m/s

the differential equation becomes,

$$\lambda c_1 \mathrm{e}^{\lambda t} = \mathbf{A} c_1 \mathrm{e}^{\lambda t}, \tag{35}$$

where by cancelling the $\mathrm{e}^{\lambda t}$ term it can be seen that λ are the eigenvalues of $\mathbf{A}$. From Eq. 34 it can be seen that, in order for the solution to decay from an initial displacement to its initial value x_0, the real parts of all eigenvalues λ must be negative.

For both symmetric and asymmetric vessel geometries, there exists an eigenvalue of $\mathbf{A}$ which has a positive real part. As a result, any perturbation will lead to unbounded deviation from the initial state.

5.4 The cost matrices **Q** and **R**

Prior to using the simulation, suitable values for the state cost and control cost matrices must be determined. Bryson [7] gives a general rule for the diagonal cost matrices. If each state and control variable has a maximum desired value of $x_i$max and $u_i$max, respectively, then:

$$Q_{ii} = \frac{1}{x_i \mathrm{max}^2} \qquad R_{ii} = \frac{1}{u_i \mathrm{max}^2} \tag{36}$$

Typical values for $x_i$max and $u_i$max are displayed in Table 2.

5.5 Integral feedback

Initial simulations indicate that the model achieves a stable steady-state result with a constant rudder angle and speed offsetting the constant attraction force and moment from the wall. When it reaches a steady state, however, the vessel has an offset from its initial separation distance. In order to minimize this steady-state drift error, an additional state variable is added. Stengel [6] discusses the addition of an integral feedback state variable in order to overcome steady-state errors.

If y is the cross-track error in the state equation as displayed in Eq. 26, we can add an additional state variable.

$$y_i = \int_0^t y(\tau)\mathrm{d}\tau, \quad \dot{y}_i(t) = y(t). \tag{37}$$

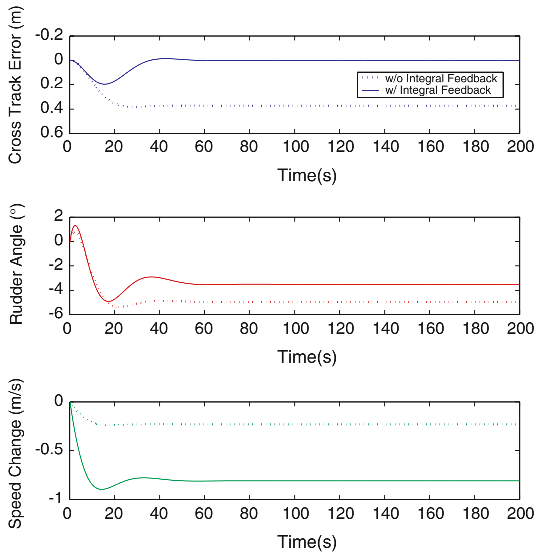

Fig. 5 Integral feedback control history comparison (Fn = 0.16, $d = 15$ m). $\mathrm{Fn} = \frac{u}{\sqrt{Lg}}$ is the Froude number

With the addition of this state variable the state equation now becomes:

$$\begin{bmatrix} \dot{U}_2 \\ \dot{\Omega}_3 \\ \dot{\psi} \\ \dot{y} \\ \dot{y}_i \end{bmatrix} = \begin{bmatrix} \mathbf{m}_{ij}^{-1} & \cdot\mathbf{b}_{ij} & 0 & 0 & 0 \\ & & 0 & 0 & 0 \\ 0 & 1 & 0 & 0 & 0 \\ 1 & 0 & U_1 & 0 & 0 \\ 0 & 0 & 0 & 1 & 0 \end{bmatrix} \begin{bmatrix} U_2 \\ \Omega_3 \\ \psi \\ y \\ y_i \end{bmatrix} + \begin{bmatrix} \mathbf{m}_{ij}^{-1} \cdot \begin{bmatrix} \frac{1}{2}\frac{\partial C_L}{\partial \delta_R}\rho S U_1^2 & C_s(d)\rho BTU_1 \\ \frac{1}{2}\frac{\partial C_L}{\partial \delta_R}\rho S U_1^2 x_T & C_m(d)\rho BTLU_1 \end{bmatrix} \\ \begin{matrix} 0 & \qquad 0 \\ 0 & \qquad 0 \\ 0 & \qquad 0 \end{matrix} \end{bmatrix} \begin{bmatrix} \delta_R \\ \delta_u \end{bmatrix}. \tag{38}$$

Implementing this new state equation eliminates the steady-state error as may be seen in Fig. 5.

5.6 Significance of viscous effects

Having developed linear expressions for viscous damping in both sway and yaw, we may determine the relative importance of these effects. $B_{22_{\mathrm{Visc}}}$ and $B_{66_{\mathrm{Visc}}}$ may be added to the state equation. This yields a new controller which has an $\mathbf{A}$ matrix and gain affected by the presence of the equivalent linear viscous terms.

$$\dot{\mathbf{x}} = [\mathbf{A} - \mathbf{BK}]_{\mathrm{Visc}}\mathbf{x}. \tag{39}$$

If the controlled system is thought of as a classical mechanical oscillator, the controller provides both a damping effect when acting on the U_2 and Ω_3 state variables, as well as restoring effect when acting on the integral state variables y and ψ. The damping and restoring effects, with or without viscous effects, may be seen though the classical analysis of such systems. The general solution to the homogeneous Eq. 39 is:

$$x(t) = c_1 \mathrm{e}^{\lambda_1 t} + c_2 \mathrm{e}^{\lambda_2 t} \tag{40}$$

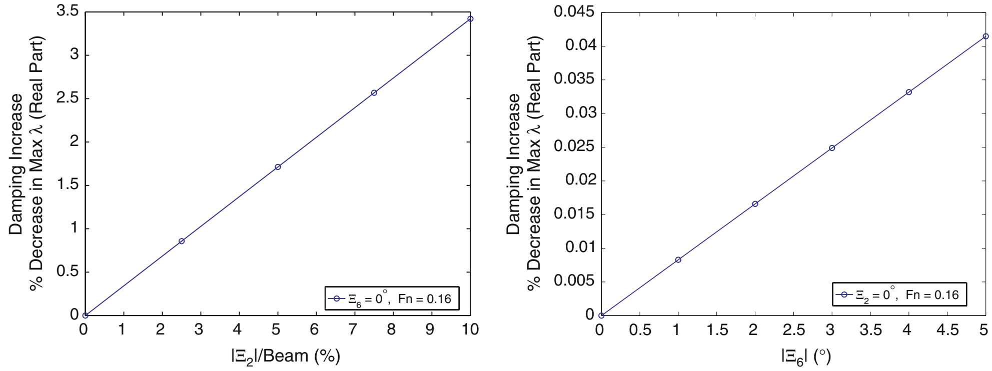

Fig. 6 Damping increase dependence on assumed sway and yaw amplitude

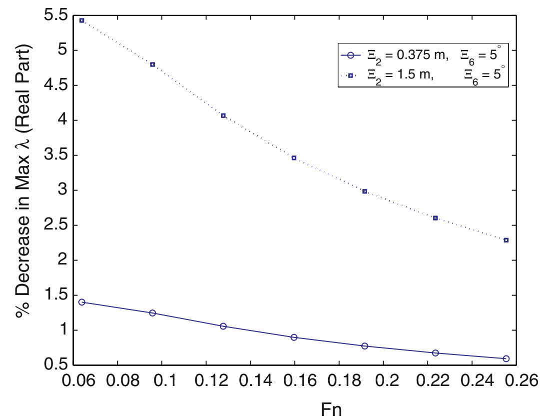

Fig. 7 Damping-increase dependence on forward speed

In general the eigenvalues (λ) may be complex of the form $(a + b\mathrm{i})$ so that the general solution becomes

$$x(t) = d_1 \mathrm{e}^{at} \cos bt + d_2 \mathrm{e}^{at} \cos bt. \tag{41}$$

Here x is considered to be a vector of oscillations about the nominal state, with frequency b and amplitude e^{at}. The eigenvalue of $[\mathbf{A} - \mathbf{BK}]_{\mathrm{Visc}}$ with the greatest real part, a, will control the damping or stability of the entire system. The viscous terms must always take energy out of the system, so viscous effects increase damping and decrease a. In order to determine the significance of this increase, the real parts of the largest (least negative) eigenvalue of $[\mathbf{A} - \mathbf{BK}]$ and $[\mathbf{A} - \mathbf{BK}]_{\mathrm{Visc}}$ are compared.

Quantifying the damping terms in Eqs. 30 and 31 requires a suitable selection of $|\Xi_2|, |\Xi_6|, \omega$ and C_D. A C_D of 1 was selected for bluff-body cross-sections. For ω the imaginary parts of the eigenvalues of $[\mathbf{A} - \mathbf{BK}]$ provide a reasonable value of 0.15 rad/s (see figure). The magnitudes of $|\Xi_2|$, $|\Xi_6|$ and forward speed are varied. Figure 6 shows that, as the sway and yaw amplitudes are allowed to increase, there is a linear increase in the damping of the controlled system.

Figure 7 shows the increase in the controlled-system damping when viscous effects are added over a range of speeds for two different sway amplitudes. Even when less-realistic sway amplitudes are considered at a low speed, the viscous effects only contribute a 5% increase to the total system damping. At more relevant amplitudes and speeds, viscous effects contribute only 1% to the total damping. These results demonstrate that control forces dominate the system performance, while viscous effects are quite small by comparison.

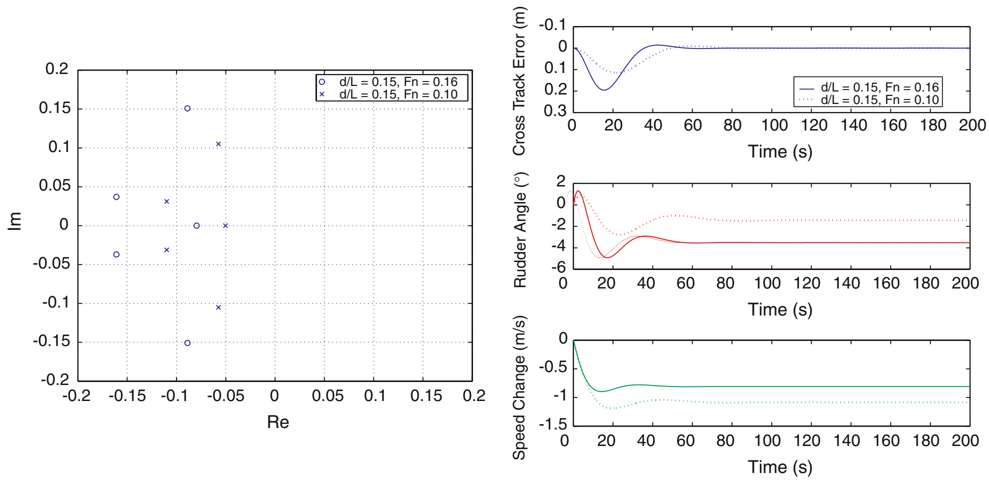

Fig. 8 [$\mathbf{A} - \mathbf{BK}$] eigenvalues and associated control history

5.7 Controlled-system stability

Simulations indicate stable behavior over a range of separation distances and speeds. Speeds ranged from Froude numbers of 0.064–0.255. Centerline to wall separation distances ranged from 10 m to 60 m. With the controller on, the stability of the system may be determined by examining the eigenvalues of [$\mathbf{A} - \mathbf{BK}$]. For the entire range of scenarios tested, the real parts of the eigenvalues for the controlled-state equation, [$\mathbf{A} - \mathbf{BK}$], are all negative, indicating stable behavior of the controlled system. Figure 8 is a plot of the eigenvalues and associated control history for the controlled system operating at two different speeds. As these figures show, changes to the initial simulation parameters of speed and separation alter the position of eigenvalues on the complex plane and thus the response of the controller. Reducing the initial forward speed and increasing the separation distance both bring the eigenvalues closer to the imaginary axis, reducing stability, and increasing the time required to reach steady state.

5.7.1 The controller's use of speed

In every case the control system chooses to reduce speed in reaching steady state. Some limitations of the controller simulation and design become clear when looking at the speed changes called for by the controller. For the minimum separation ($d/L = 0.1$), the speed reduction is greater than 10% at all initial speeds and should not be considered small.

5.7.2 The controller's use of rudder

For every scenario simulated the controller achieves a steady-state rudder angle. In general, this steady-state rudder angle is negative. A rudder angle which should turn the vessel towards the wall is perhaps counter intuitive at first.

Looking back to Eq. 8, there is a term in the moment equation that, when taken alone, becomes

$$M_3 = U_1 U_2 (m_{11} - m_{22}). \tag{42}$$

Considering the heading angle ψ, the equation becomes:

$$M_3 = -U^2 \sin(\psi)\cos(\psi)(m_{11} - m_{22}). \tag{43}$$

For long slender bodies $(m_{11} - m_{22}) < 0$, so the moment is positive in sign and destabilizing in general. This effect is known as the "Munk Moment".

In order to overcome the suction due to the wall on the starboard side, the control system turns the ship to port a small amount, known generally as a crab angle. With the small but steady negative heading angle, a negative Munk moment is present and so the controller must counteract this with a negative rudder angle. Here again, as separation grows large, the required rudder angle diminishes. An analogous study involving the seakeeping, motion control and stability of high-speed hydrofoil vessels using a similar LQ controller is presented in [8].

6 Conclusion

Applying modern optimal-control theory it has been shown that the hydrodynamic-interaction effects of a ship with a vertical wall or similar vessel on a parallel course may be mitigated and controlled in real time by the active regulation of the rudder angle, ship speed as well as their rates of change. The controller strikes a careful balance between interaction, control and maneuvering forces on the vessel in order to reach a stable and an a priori specified steady state. Viscous forces have been estimated through equivalent linearization. When the damping effects of these viscous terms are compared to the damping effects induced by the controller, it is clear that the physical viscous effects are insignificant and may be neglected.

The present study presents an example of the promise underlying the development of intersections between theoretical and numerical marine hydrodynamics and modern optimal-control theory for the development of active vessel-response-regulation algorithms of significant interest in practice.

References

1. Lewis EV (ed) (1989) Principles of naval architecture, 2nd edn, volume III. Society of Naval Architects and Marine Engineers
2. Vantorre M, Laforce E, Verzhbitskaya E (2001) Model test based formulations of ship–ship interactions forces for simulation purposes. In: International Marine Simulator Forum
3. Tuck EO, Newman JN (1974) Hydrodynamic interactions between ships. In: Proceedings for the 10th symposium on naval hydrodynamics, pp 35–70
4. Sclavounos PD, Purvin S, Talha U, Kim S (2003) Simulation based resistance and seakeeping performance of high-speed monohull and multihull vessels equipped with motion control lifting appendages. In: Keynote Lecture, FAST 2003 Conference, Ischia Italy
5. Newman JN (1977) Marine hydrodynamics. The MIT Press
6. Stengel RF (1994) Optimal control and estimation. Dover
7. Bryson AE, Ho Y (1975) Applied optimal control. Hemisphere Publishing
8. Chatzakis II, Sclavounos PD (2005) Active control of a high-speed hydrofoil vessel using state-space methods. J Ship Res